Polyhedron 243 (2023) 116572

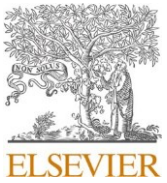

Contents lists available at ScienceDirect

Polyhedron

journal homepage: www.elsevier.com/locate/poly

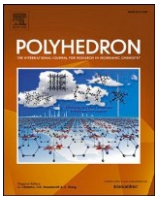

Chemical bonding in lead anionic clusters

Anton S. Pozdeev, Alexander I. Boldyrev *, Yi Rao *

Department of Chemistry and Biochemistry, Utah State University, 0300 Old Main Hill, Logan, UT 84322, United States

ARTICLE INFO

Keywords:
Lead
AdNDP
Zintl anions
Bonding analysis
Aromaticity

ABSTRACT

Lead anion clusters, as examples of Zintl anions, have captivated researchers due to their intriguing structures and unexpected stoichiometries. Despite extensive experimental and theoretical investigations, the understanding of the chemical bonding in these clusters remains incomplete and subject to interpretation. In this study, we focused on several widely studied homoatomic and heteroatomic lead anionic clusters and employed the Adaptive Natural Density Partitioning (AdNDP) algorithm to decipher their bonding patterns. Our aim was to provide chemically intuitive descriptions of the bonding in these clusters. Our findings reveal the presence of multiple delocalized bonds in most of the studied lead clusters. Remarkably, these bonding patterns exhibit characteristics of aromatic compounds. This work represents a step towards a more comprehensive understanding of the bonding in lead anion clusters. By shedding light on their chemical bonding patterns, we hope to inspire further research in the design and synthesis of novel lead homoatomic and heteroatomic Zintl clusters, fostering advancements in their properties and potential applications.

1. Introduction

Metallic polyanion clusters have been the subject of extensive theoretical and experimental investigations for over a century [1]. Among them, the most remarkable and famous species are Zintl anions, including those of formulae $[E_{10}]^{2-}$, $[E_9]^{4-}$ $[E_5]^{2-}$ and many others, where E is silicon, germanium, tin, and lead for Group 14. The first known Zintl anion, NaPb, was obtained in 1891 and later found to contain Pb_9^{4-} anion [2–4]. These clusters predominantly consist of heavy p-elements and exhibit non-classical multi-center bonds; thus, their bonding patterns are quite remarkable since the properties of atomic clusters lie between those of single atoms and the bulk.

Lead, being the heaviest stable element in Group 14, demonstrates rich and varied experimentally investigated cluster chemistry. The smallest found cluster is $[Pb_4]^{4-}$ [4]; also, it includes $[Pb_5]^{2-}$ [5], $[Pb_9]^{4-}$ [6], and $[Pb_{10}]^{2-}$ [7] as examples of homoatomic clusters, $[Pb_9\text{-Cd-Cd-}Pb_9]^{6-}$, [8] $[Ni@Pb_{10}]^{2-}$ [9], $[Cu@Pb_9]^{3-}$ [10] and many others [11] as representatives of heteroatomic lead clusters. The synthesis and common properties of these lead clusters are extensively described in various sources [11–15]; moreover, the structures of most clusters are often well-confirmed by the predictions of Wade's rules [11,14,16]. However, there is still a lack of understanding of chemical bonding in such species.

In this study, we applied the Adaptive Natural Density Partitioning (AdNDP) method [17] to investigate the bonding patterns of lead clusters. Traditional analyses based on canonical molecular orbitals often fail to provide accurate results for these structures due to the presence of aromatic, non-aromatic, and non-bonding patterns within the same orbital. The AdNDP method overcomes this limitation by identifying Lewis's bonding elements, including 1c-2e lone pairs and 2c-2e classical bonds, as well as non-classical multi-center (delocalized) bonds known as mn-2e bonds, where $m \geq 3$. This approach was earlier applied to decipher the chemical bonding patterns of molecules [18–20], Aluminum clusters [21,22], Germanium clusters [24,25], and many others [23,26–30]. The concept of aromaticity apart from classical treatment for organic molecules [31,32] can be also successfully applied to inorganic structures, for example, Boron cluster [33,34], metal clusters [35–38], metalbenzene [39], etc. This description includes both π- and σ-aromaticity. The AdNDP method allows to introduce the concepts of aromaticity naturally. In this work, we utilize the AdNDP method to explore and describe the aromaticity in the lead anionic clusters.

2. Theoretical method

For geometry optimization we chose two DFT functionals - Tao-Perdew-Staroverov-Scuseria (TPSSh) [40] and Perdew–Burke-Ernzerhof (PBE0) [41]. TPSSh was selected for its balance of speed and accuracy, while PBE0 is a commonly used functional for DFT calculations of main group elements. For all calculations we used def2-TZVPPD basis

* Corresponding authors.
E-mail addresses: a.i.boldyrev@usu.edu (A.I. Boldyrev), yi.rao@usu.edu (Y. Rao).

https://doi.org/10.1016/j.poly.2023.116572
Received 22 May 2023; Accepted 20 July 2023
Available online 25 July 2023

set [42–44] in conjunction with the scalar-relativistic effective core potential def2-ECP [42] using ORCA 5.03 software [45,46]. The frequency calculations were performed at the same level of theory, none of the clusters except $[Pb_9]^{4-}$ (C_{4v}) have imaginary frequencies. The singlet state was considered for all investigated structures, while choosing triplet state leads to reduction of symmetry for most stoichiometries and significant increase in energy. Chemical bonding patterns were analyzed using the AdNDP algorithm [17] as implemented in AdNDP 2.0 code written by Tkachenko [47]. This method is based on the concept of an electron pair as the main bonding element; the algorithm involves to the partitioning of the electron density into elements with the lowest symmetry-appropriate number of atomic centers per electron pair, which allows us to represent an electronic structure as *n*-center two-electron bonds (nc-2e, n is a number of atoms participating in the bond) in the RHF formalism and *n*-center one-electron bonds in the UHF formalism. The density matrices were obtained at TPSSh/def2-TZVPPD level of theory.

It's important to emphasize that studied multiply charged lead anions are predominantly identified in the solid phased or solutions in the presence of counter cations. They are not stable on their own and presented calculations are a model used for bonding deciphering of isolated lead clusters. The ChemCraft software was used for visualization of the structures and AdNDP orbitals [58].

3. Discussions

3.1. Homoatomic lead clusters

In this section, we discuss bonding pattern and structural features of experimentally investigated Pb polyanionic clusters, namely $[Pb_4]^{4-}$, $[Pb_5]^{2-}$, $[Pb_9]^{4-}$, $[Pb_{10}]^{2-}$, and $[Pb_{12}]^{2-}$. All structures were optimized at PBE0/def2-TZVPPD and TPSSh/def2-TZVPPD levels of theory, XYZ coordinates are presented in Tables S1 and S2 (SI). We found no differences of any significance between structures obtained at the two level of theory; we chose TPSSh geometries as a reference for this work.

3.1.1. $[Pb_4]^{4}$

We start with the analysis of $[Pb_4]^{4-}$, the smallest polyanion cluster. The optimized structure of the isolated cluster exhibits T_d symmetry (Fig. 1), which is consistent with the Rb_4Pb_4 phase reported in ref. [48].

The 20 valence electrons can be localized into four 1c-2e lone pairs with an occupancy number (ON) of 1.99e and six 2c-2e σ-bonds with ON = 1.99e. Therefore, the bonding in this cluster consists solely of classical bonding elements. Therefore, this cluster can be adequately described in terms of classical bonding elements, and we classify it as a classical structure. Interesting, that stability of this compound is possible to explain in terms of the Hirsch rule of 3D aromaticity as discussed in ref. [49,50].

3.1.2. $[Pb_5]^{2}$

The $[Pb_5]^{2-}$ cluster has been identified as a D_{3h} trigonal bipyramidal cluster in $[Na([2.2.2]crypt)]_2Pb_5$ phase [5]. The same motif was found in the DFT calculations (Fig. 2). We found two alternative AdNDP bonding patterns. The 22 valence electron can be localized into five 1c-2e lone pairs with ON = 1.97e (not shown in the Figure), the remaining 12 electrons can be localized into either six 3c-2e bonds (Fig. 2C) with an ON = 1.98e on each face of the bipyramid, or six 4c-2e bonds (Fig. 2D) with ON = 1.99e-1.97e, with three bonds located on each Pb_4 pyramidal fragment. Anyway, both approaches introduce delocalized multi-center bonds, i.e., we classify the structure as non-classical.

3.1.3. $[Pb_9]^{4}$

The $[Pb_9]^{4-}$ cluster demonstrates structural flexibility and can adopt different geometries. Generally, the $[E_9]^{4-}$ motif is observed for many elements. For example, $[Ge_9]^{4-}$ was found as a C_{4v} structure (capped antiprism) in the Cs_4Ge_9 phase [51], whereas $[Sn_9]^{4-}$ was identified as close to tricapped D_{3h} symmetry trigonal prism in the $[K([18]crown-6)]_3K$-$[Sn_9]$ phase [52]. $[Pb_9]^{4-}$, the cluster of our interest, was investigated as a C_{4v} motif in the $[K(18\text{-crown-}_6)]_4[Pb_9]$*en*tol phase [53]; however, for the isolated species the C_{4v} geometry has one imaginary frequency, while the tricapped trigonal prism of D_{3h} symmetry is found to be a minimum on PES what contradicts the predictions of the Wade's rule. Thus, we decided to investigate both possible geometries for $[Pb_9]^{4-}$.

For the capped square antiprism (C_{4v} symmetry, Fig. 3) the 40 valence electrons can be localized into nine 1c-2e lone pairs with ON = 1.93, then the remaining 22 electrons form three aromatic areas in the cluster. The base of Pb_8 antiprism has three 4c-2e σ-bonds with ON = 1.98–1.68e (the first area), the Pb_5 cap has three 5c-2e σ-bonds with ON = 1.99–1.94e (the second area), remaining electrons form five 8c-2e σ-bonds within the Pb_8 antiprism fragment (the thirds area).

In the tricapped trigonal prismatic structure (D_{3h}, Fig. 4) we localized the 40 valence electrons into nine 1c-2e lone pairs with ON = 1.96–1.94e, two 3c-2e σ-bonds with ON = 1.96–1.94e located at both sides of the trigonal prism, and nine 5c-2e σ-bonds, where three bonds located on each Pb_5 cap. We classify these Pb_5 caps as three separate σ-aromatic fragments. Ref. [49] explores the stability of the D_{3h} geometry and attributes it to the presence of a double spherically aromatic configuration in the valence-electron system. This configuration encompasses 32 σ electrons ($N_\sigma = 3$) and 8 π electrons ($N_\pi = 1$), satisfying Hirsch's $2(N + 1)^2$ rule. The fulfillment of this rule contributes to the enhanced stability observed in the D_{3h} geometry.

Thus, both structures of C_{4v} and D_{3h} symmetry have multiple delocalized bonds Interesting, similar AdNDP patterns were found for

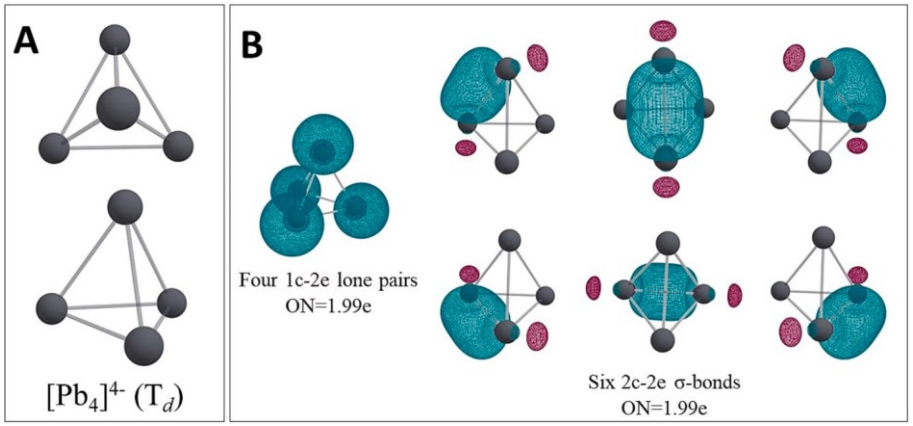

Fig. 1. **A** — Optimized geometry of $[Pb_4]^{4-}$ (T_d) in two projections, **B** — AdNDP chemical bonding pattern.

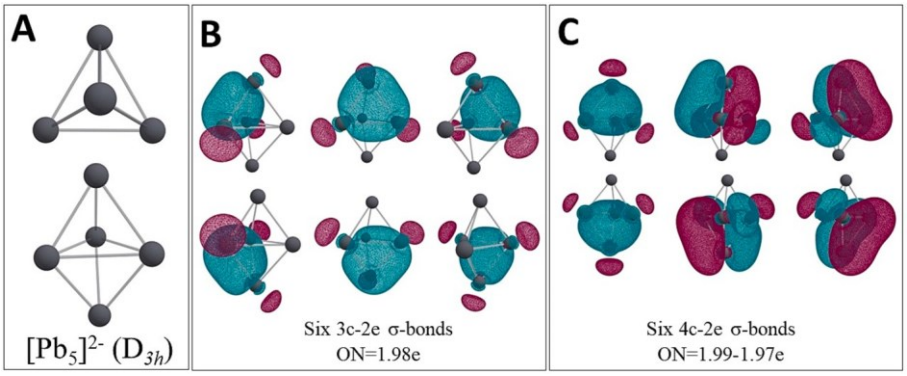

Fig. 2. **A** — Optimized geometry of $[Pb_5]^{2-}$ (D_{3h}) in two projections, **B** and **C** — two alternative AdNDP chemical bonding patterns.

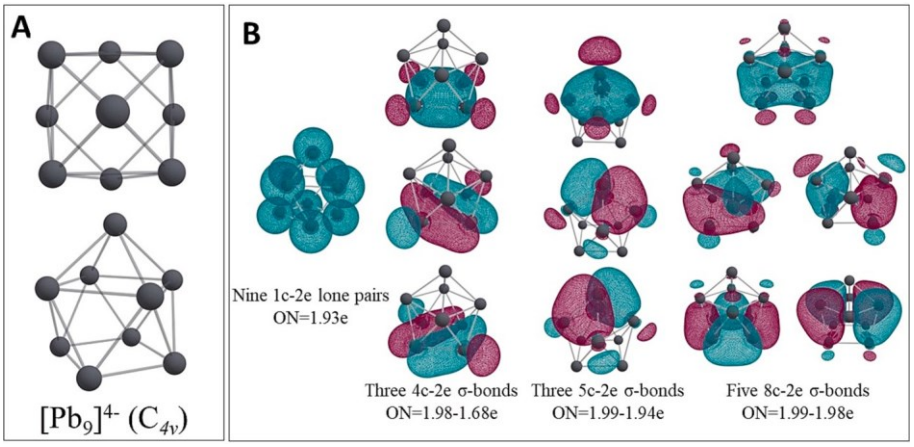

Fig. 3. **A** — Optimized geometry of $[Pb_9]^{4-}$ (C_{4v}) in two projections, **B** — AdNDP chemical bonding pattern.

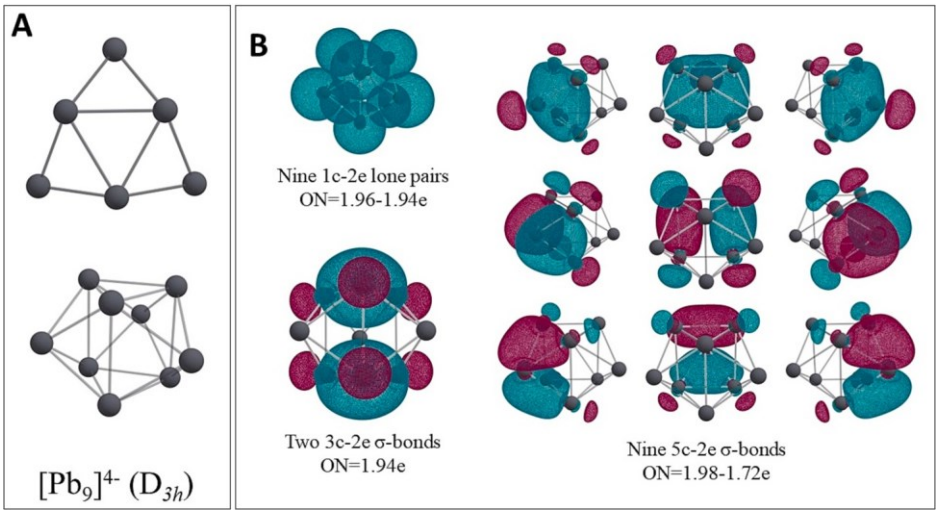

Fig. 4. **A** — Optimized geometry of $[Pb_9]^{4-}$ (D_{3h}) in two projections, **B** — AdNDP chemical bonding pattern.

$[Ge_9]^{4-}$ earlier [54].

3.1.4. $[Pb_{10}]^2$

$[Pb_{10}]^{2-}$ is quite a rare lead cluster. It was observed in the K([2.2.2] crypt)]$_2$Pb$_{10}$ phase as a D_{4d} bicapped square antiprism [7]. We found that this geometry pattern is also stable for an isolated cluster (Fig. 5). This structure can be described as a further derivative of $[Pb_9]^{4-}$, so one would expect a similar AdNDP bonding pattern.

We localized the 42 valence electrons into ten 1c-2e lone pairs with ON = 1.96–1.94e; other found delocalized bonds resemble those of $[Pb_9]^{4-}$. Two opposite caps of Pb_5 possess six 5c-2e σ-bonds (the same motif was found for the Pb_5 cap of $[Pb_9]^{4-}$), the remaining electrons form five 8c-2e σ-bonds within the Pb_8 antiprism how it was found for the $[Pb_9]^{4-}$ cluster.

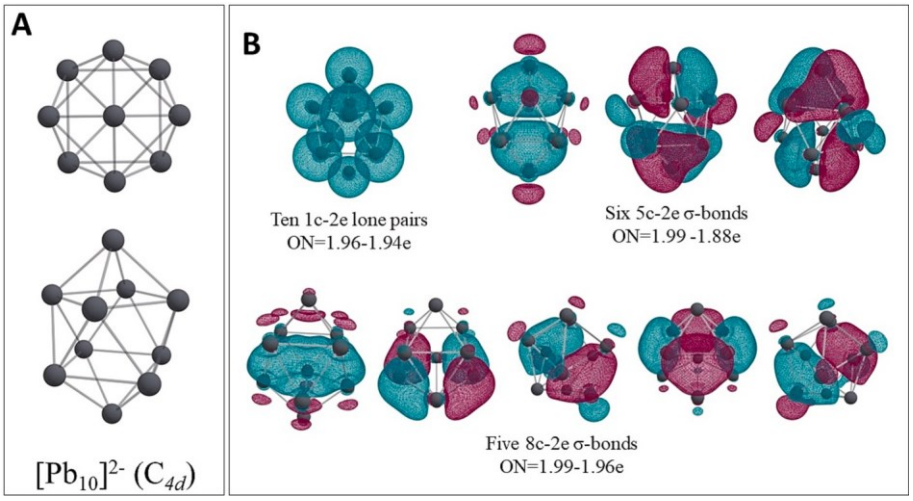

Fig. 5. **A** — Optimized geometry of $[Pb_{10}]^{2-}$ (C_{4d}) in two projections, **B** — AdNDP chemical bonding pattern.

3.1.5. *[Pb12]2*

The $[Pb_{12}]^{2-}$ cluster, also known as plumbaspherene, was recently discovered in gas phase through photoelectron spectroscopic (PES) experiments [55]. It was found to possess a high symmetrical I_h structure. In the original paper the bonding was described in terms of bonds delocalized between all twelve atoms. They are composed of p-orbitals, what is based on the shape of canonical MO. The approach is natural and rational. Nevertheless, we suggest an alternative AdNDP bonding pattern where we describe the cluster as a bicapped derivative of pentagonal antiprism (Fig. 6). This approach was found to be quite suitable for description of the $[Pb_{10}]^{2-}$, $[Pb_9]^{4-}$ (C_{4v}) clusters, and some heteroatomic lead clusters.

Using the AdNDP method, we found twelve 1c-2e lone-pairs with ON = 1.94e; two Pb_6 caps located on opposite sides possess three 5c-2e bonds with ON = 1.99–1.93e; remaining electrons form seven 10c-2e with ON = 1.99–1.92 eV within the pentagonal antiprism framework. Regardless of the approach, delocalized orbitals should be introduced for bonding description of plumbaspherene. As in the cases of $[Pb_9]^{4-}$ (and $[Pb_{10}]^{2-}$) we found several aromatic fragments.

3.2. Heteroatomic lead clusters

According to AdNDP analysis all studied clusters, starting from $[Pb_5]^{2-}$, exhibit non-classical delocalized bonds and can be classified as aromatic compounds. It is important to note that the described bonding patterns are not unique, and alternative bonding schemes may exist. However, in this study, the aim was to provide a self-consistent description of the structures using the AdNDP approach. In addition to the lead clusters discussed earlier, the current section also includes several examples of heteroatomic lead clusters. These examples further support the proposed approach and demonstrate its applicability to various types of lead-containing compounds.

3.2.1. *[Cu@Pb9]3*

A well-ordered $[Cu@Pb_9]^{3-}$ cluster with D_{3h} symmetry is observed in the $[K([2.2.2]crypt)]_3[Cu@Pb_9](dmf)_2$ phase [10] and confirmed by DFT calculations (Fig. 7). Thus, we can describe this centered tricapped trigonal prismatic structure as a derivative of the previously discussed $[Pb_9]^{4-}$ cluster of D_{3h} symmetry. According to the AdNDP analysis, the cluster has five 1c-2e 3d lone pairs on the copper atom with ON = 1.92–1.98e (omitted from the Fig. 7) and nine 1c-2e lone pairs with ON = 1.93–1.91e on lead atoms; both bases of the trigonal prism have two 3c-2e σ-bonds with ON = 1.92e. The copper atom participates in nine 6c-2e bonds with ON = 1.98–1.92e, three of which are located on each Pb_5 cap. Thus, the found AdNDP orbitals are very similar to those of $[Pb_9]^{4-}$, where the copper atom is naturally incorporated in the 5c-2e bonds of

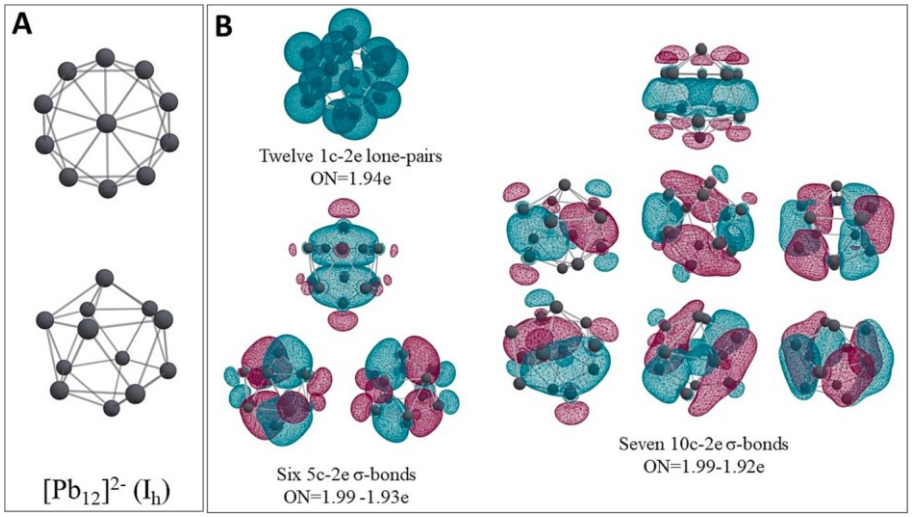

Fig. 6. **A** — Optimized geometry of $[Pb_{12}]^{2-}$ (I_h) in two projections, **B** — AdNDP chemical bonding pattern.

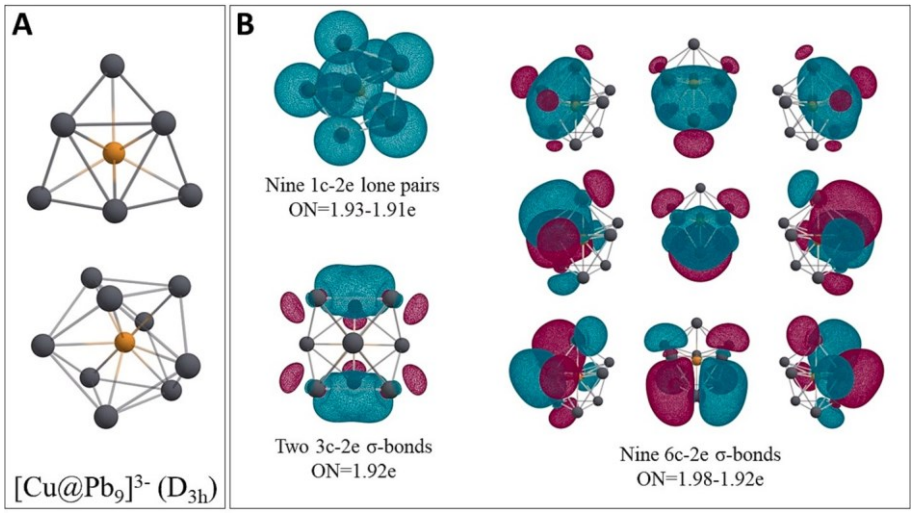

Fig. 7. **A** — Optimized geometry of $[Cu@Pb_9]^{3-}$ (D_{3h}) in two projections, **B** — AdNDP chemical bonding pattern.

each Pb_5 fragments. The AdNDP analysis provides insights into the bonding nature of the $[Cu@Pb_9]^{3-}$ cluster and highlights its relationship to the $[Pb_9]^{4-}$ cluster, with the incorporation of the copper atom into the bonding framework. This analysis enhances our understanding of the cluster's electronic structure and bonding characteristics.

3.2.2. *[Ni@Pb10]2*

The $[Ni@Pb_{10}]^{2-}$ cluster of D_{4d} symmetry (according to the DFT calculation, Fig. 8) is an example of endohedral clusters where one nickel atom is incorporated into the center of $[Pb_{10}]^{2-}$ bicapped square antiprism; the same geometry was observed in the $[K([2.2.2]crypt)]_2[Ni@Pb_{10}]$ phase [9]. Based on this structural similarity, we can expect to find AdNDP bonding pattern similar to that of $[Pb_{10}]^{2-}$.

We found five 1c-2e 3d lone pairs on the nickel atom (omitted from Fig. 8) and ten 1c-2e lone pairs on all lead atoms. Both Pb_5 cap fragments possess six 5c-2e σ-bonds with ON = 1.98–1.84e. The remaining electrons form five 9c-2e bonds of the Pb_8 antiprism with the incorporated nickel atom with ON = 1.99–1.95e. The influence of Ni atom from 5 to 20% in the 9c-2e orbitals, thus it is naturally included in the bonding picture of the $[Pb_{10}]^{2-}$ cluster.

3.2.3. *[Pb9-Cd-Cd-Pb9]6*

The $[Pb_9\text{-}Cd\text{-}Cd\text{-}Pb_9]^{6-}$ cluster with pseudo-D_{4h} symmetry was identified in the $[K([2.2.2]crypt)]_6[Pb_9\text{-}Cd\text{-}Cd\text{-}Pb_9](en)_2$ phase [8]. It can be described as two Pb_9Cd fragments conjugated to each other via Cd-Cd bond. A similar structure was obtained via DFT (Fig. 9). The ideal D_{4d} symmetry has one imaginary frequency leading to rotation of one Pb_9 group to rotate towards the second Pb_9 group.

According to the AdNDP analysis, there are eighteen 1c-2e lone pairs with ON = 1.95–1.91e on each Pb atom, ten 1c-2e lone pairs with ON = 1.99e on both Cd atoms (all of them are omitted from the Fig. 9), and one 2c-2e Cd-Cd σ-bond with ON = 1.92e. Other found delocilzed bonds are similar to those of $[Pb_{10}]^{2-}$ and $[Pb_9]^{4-}$ clusters, i.e., six 5c-2e Pb-Pb-Pb-Pb-Pb σ-bonds with ON = 1.99–1.92e located on two opposite Pb_5 caps of $[Pb_9\text{-}Cd\text{-}Cd\text{-}Pb_9]^{6-}$; six 5c-2e Cd-Pb-Pb-Pb-Pb σ-bonds with ON = 1.99–1.92e located on two Pb_4Cd caps; the remaining electrons are localized into ten 8c-2e with ON = 1.99–1.85e within both Pb_8 antiprism fragments.

Indeed, the $[Pb_9\text{-}Cd\text{-}Cd\text{-}Pb_9]^{6-}$ cluster exhibits dual aromaticity, indicating the presence of two aromatic units within the cluster. This feature is reminiscent of the original $[Pb_9]^{4-}$ cluster with C_{4v} symmetry. The concept of dual aromaticity, where multiple aromatic units coexist within a single molecular system, has been investigated in previous studies, for example, in ref. [56]. This investigation contributes to our broader understanding of aromaticity and its implications in various chemical systems.

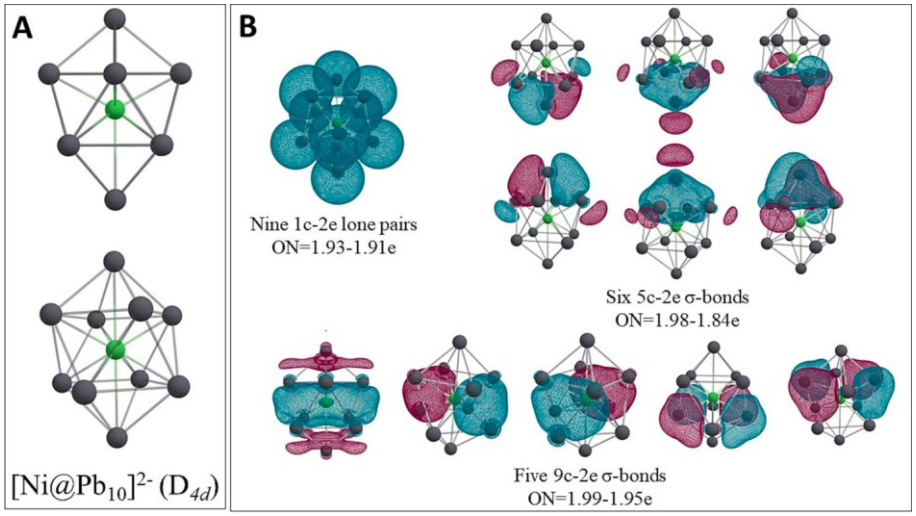

Fig. 8. **A** — Optimized geometry of $[Ni@Pb_{10}]^{2-}$ (D_{4d}) in two projections, **B** — AdNDP chemical bonding pattern.

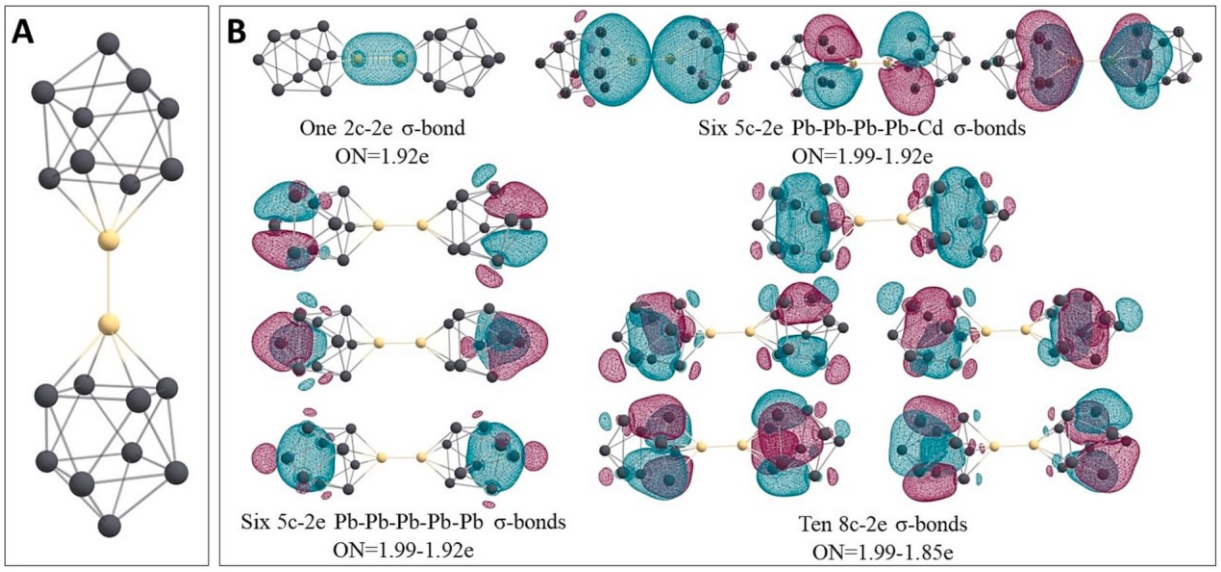

Fig. 9. **A** — Optimized geometry of $[Pb_9\text{-}Cd\text{-}Cd\text{-}Pb_9]^{6-}$, B — AdNDP chemical bonding pattern.

3.2.4. $[Pb_{12}Rh]^3$

The $[Pb_{12}Rh]^{3-}$, belonging to the $[M@Pb_{12}]^{3-}$ (M = Co, Rh, Ir) series, has been characterized in ref. [56,57]. For the isolated species we found I_h symmetry (Fig. 10) what allows to describe the structure as a heteroatomic derivative of the $[Pb_{12}]^{2-}$ cluster.

We found AdNDP bonds close to those of the $[Pb_{12}]^{2-}$ cluster. Two approaches were initially considered: delocalized 13c-2e bonds and the description of the structure as a bicapped pentagonal antiprism. Both approaches yielded bonding patterns that were similar to each other, and the latter approach was chosen to maintain consistency with the bonding analysis of lead Zintl anions in this study. We found twelve 1c-2e lone pairs with ON = 1.91e on each Pb atom, five 1c-2e lone pairs with ON = 1.87e on the Rh atom (omitted from the Fig. 10). Also, it possesses six 5c-2e σ-bonds with ON = 1.99–1.96e on two Pb_5 caps and seven 11c-2e σ-bonds with ON = 1.99e within the Pb_8Rh centered antiprism.

Indeed, the application of the AdNDP algorithm has allowed for the natural and consistent description of bonding patterns in selected homoatomic lead clusters and their heteroatomic derivatives. By employing this approach, similarities in the bonding patterns have been identified, showcasing a structural evolution through the introduction of similar delocalized bonds.

4. Conclusion remarks

We conducted an AdNDP chemical bonding analysis on various homoatomic and heteroatomic lead anionic clusters. Our analysis revealed that all lead atoms in these structures retain their lone pairs, resulting in bond formation primarily involving p-orbitals. The stability of these clusters can be attributed to the presence of local σ-aromaticity, which supports their overall structural integrity. Importantly, the bonding patterns identified for homoatomic lead clusters were found to be applicable in describing the bonding in heteroatomic lead clusters, with the heteroatom naturally incorporated into the multi-center bonds.

Declaration of Competing Interest

The authors declare that they have no known competing financial interests or personal relationships that could have appeared to influence the work reported in this paper.

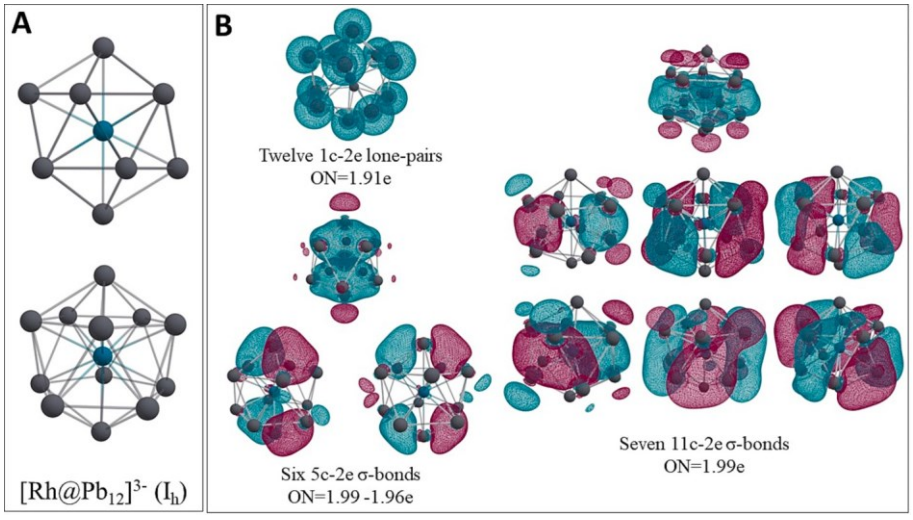

Fig. 10. **A** — Optimized geometry of $[Rh@Pb_{12}]^{2-}$ (I_h) in two projections, **B** — AdNDP chemical bonding pattern.

Data availability

Data will be made available on request.

Acknowledgements

Y.R. was supported by the National Science Foundation under Grant No. [2045084]. The support and resources from the Centre for High-Performance Computing at the University of Utah are gratefully acknowledged. A.I.B. acknowledges financial support from the R. Gaurth Hansen Professorship fund.

Appendix A. Supplementary data

Supplementary data to this article can be found online at https://doi.org/10.1016/j.poly.2023.116572.

References

[1] M. Joannis, Hebd. Seances Acad. Sci. 113 (1891) 795.
[2] L. Diehl, K. Khodadadeh, D. Kummer, J. Stra¨hle, Chem. Ber. 109 (1976) 3404–3418.
[3] E. Zintl, A. Harder, Z. Phys, Chem. Abt. A 154 (1931) 47.
[4] R.E. Marsh, D.P. Shoemaker, Acta Cryst. 6 (1953) 197–205.
[5] P.A. Edwards, J.D. Corbett, Inorg. Chem. 16 (1977) 903–907.
[6] E. Todorov, S.C. Sevov, Inorg. Chem. 37 (1998) 3889–3891.
[7] A. Spiekermann, S.D. Hoffmann, T.F. Fa¨ssler, Angew. Chem. Int. Ed. 45 (2006) 3459–3462.
[8] B. Zhou, M.S. Denning, T.A.D. Chapman, J.E. McGrady, J.M. Goicoechea, Chem. Commun. (2009) 7221.
[9] E.N. Esenturk, J. Fettinger, B. Eichhorn, Chem. Commun. (2005) 247.
[10] S. Scharfe, T.F. Fa¨ssler, S. Stegmaier, S.D. Hoffmann, K. Ruhland, Chem. Eur. J. 14 (2008) 4479–4483.
[11] S. Scharfe, F. Kraus, S. Stegmaier, A. Schier, T.F. F¨assler, Angew. Chem. Int. Ed. 50 (2011) 3630–3670.
[12] P. Jena, Q. Sun, Chem. Rev. 118 (2018) 5755–5870.
[13] M. Swad´zba-Kwa´sny, in: Encyclopedia of Inorganic and BioInorganic Chemistry, John Wiley & Sons Ltd, Chichester, UK, 2015, pp. 1–24.
[14] J. Campbell, D.A. Dixon, H.P.A. Mercier, G.J. Schrobilgen, Inorg. Chem. 34 (1995) 5798–5809.
[15] J. Campbell, H.P.A. Mercier, H. Franke, D.P. Santry, D.A. Dixon, G.J. Schrobilgen, Inorg. Chem. 41 (2002) 86–107.
[16] K. Wade, J. Chem. Soc. D (1971) 792.
[17] D.Y. Zubarev, A.I. Boldyrev, Phys. Chem. Chem. Phys. 10 (2008) 5207.
[18] P. Das, P.K. Chattaraj, Atoms 9 (2021) 65.
[19] H. Wang, P. Wu, Z. Wu, L. Shi, L. Cheng, Phys. Chem. Chem. Phys. 24 (2022) 17679–17685.
[20] A.S. Pozdeev, A.I. Boldyrev, Inorg. Chem. 2023 (62) (2023) 8019–8026.
[21] L. Wen, G. Li, L.M. Yang, H. Pan, E. Ganz, Mater. Today Commun. 24 (2020), 100914.
[22] S. Guin, S.R. Ghosh, A.D. Jana, J Mol Model 24 (2018) 344.
[23] C. Romanescu, T.R. Galeev, W.-L. Li, A.I. Boldyrev, L.-S. Wang, Acc. Chem. Res. 46 (2013) 350–358.
[24] N.V. Tkachenko, W.-X. Chen, H.W.T. Morgan, A. Mun˜oz-Castro, A.I. Boldyrev, Z.-M. Sun, Chem. Commun. 58 (2022) 6223–6226.
[25] Y.-S. Huang, Y. Xue, A. Mun˜oz-Castro, I.A. Popov, Z.-M. Sun, Chem. – A, Eur. J. 28 (2022) e202202192.
[26] Y. Zhang, W. Zhao, J. Lu, Y. Zhang, H. Zhang, X. Li, J. Mol. Liq. 370 (2023), 120968.
[27] Y.-H. Liao, J. Guo, P.-J. Deng, W. Dai, L. Zeng, B.-C. Zhu, J. Clust. Sci. 33 (2022) 1093–1101.
[28] J.-C. Guo, L.-Y. Feng, J. Barroso, G. Merino, H.-J. Zhai, Chem. Commun. 56 (2020) 8305–8308.
[29] J.-C. Guo, L.-Y. Feng, Y.-J. Wang, S. Jalife, A. Va´squez-Espinal, J.L. Cabellos, S. Pan, G. Merino, H.-J. Zhai, Angew. Chem. Int. Ed. 56 (2017) 10174–10177.
[30] A.S. Pozdeev, P. Rublev, A.I. Boldyrev, Y. Rao, ChemPhysChem n/a (n.d.) e202300332.
[31] E. Hückel, Z. Physik 76 (1932) 628–648.
[32] E. Hückel, Z. Physik 70 (1931) 204–286.
[33] A.S. Pozdeev, W.-J. Chen, H.W. Choi, M. Kulichenko, D.-F. Yuan, A.I. Boldyrev, L.-S. Wang, J. Phys. Chem. A 127 (2023) 4888–4896.
[34] A.P. Sergeeva, I.A. Popov, Z.A. Piazza, W.-L. Li, C. Romanescu, L.-S. Wang, A. I. Boldyrev, Acc. Chem. Res. 47 (2014) 1349–1358.
[35] Z.-L. Wang, T.-T. Chen, W.-J. Chen, W.-L. Li, J. Zhao, X.-L. Jiang, J. Li, L.-S. Wang, H.-S. Hu, Chem. Sci. 13 (2022) 10082–10094.
[36] A.J. Kalita, K. Sarmah, F. Yashmin, R.R. Borah, I. Baruah, R.P. Deka, A.K. Guha, Sci. Rep. 12 (2022) 10041.
[37] P. Rublev, N.V. Tkachenko, A.S. Pozdeev, A.I. Boldyrev, Dalton Trans. 52 (2023) 29–36.
[38] A.S. Pozdeev, P. Rublev, S. Scheiner, A.I. Boldyrev, Molecules 28 (2022) 183.
[39] I. Fern´andez, G. Frenking, G. Merino, Chem. Soc. Rev. 44 (2015) 6452–6463.
[40] J. Tao, J.P. Perdew, V.N. Staroverov, G.E. Scuseria, Phys. Rev. Lett. 91 (2003), 146401.
[41] J.P. Perdew, K. Burke, M. Ernzerhof, Phys. Rev. Lett. 77 (1996) 3865–3868.
[42] B. Metz, H. Stoll, M. Dolg, J. Chem. Phys. 113 (2000) 2563–2569.
[43] F. Weigend, R. Ahlrichs, Phys. Chem. Chem. Phys. 7 (2005) 3297.
[44] D. Rappoport, F. Furche, J. Chem. Phys. 133 (2010), 134105.
[45] F. Neese, Wiley Interdiscip. Rev. Comput. Mol. Sci 2 (n.d.) 73–78.
[46] F. Neese, WIREs Comput. Mol. Sci. 12 (2022).
[47] N.V. Tkachenko, A.I. Boldyrev, Phys. Chem. Chem. Phys. 21 (2019) 9590–9596.
[48] K. Wiesler, K. Brandl, A. Fleischmann, N. Korber, Z. Anorg, Allg. Chem. 635 (2009) 508–512.
[49] C. Liu, I.A. Popov, Z. Chen, A.I. Boldyrev, Z. Sun, Chem. Eur. J. 24 (2018) 14583–14597.
[50] A. Hirsch, Z. Chen, H. Jiao, Angew. Chem. 113 (2001) 2916–2920.
[51] V. Queneau, S.C. Sevov, Angew. Chem. Int. Ed. 36 (1997).
[52] T.F. Fassler, R. Hoffmann, Angew. Chem. Int. Ed. 38 (1999).
[53] T.F. F¨assler, R. Hoffmann, J. Chem. Soc., Dalton Trans. (1999) 3339–3340.
[54] N.V. Tkachenko, A.I. Boldyrev, Chem. Sci. 10 (2019) 5761–5765.
[55] L.-F. Cui, X. Huang, L.-M. Wang, J. Li, L.-S. Wang, J. Phys. Chem. A 110 (2006) 10169–10172.
[56] A. Mun˜oz-Castro, ChemPhysChem 21 (2020) 1384–1387.
[57] A. Li, Y. Wang, D.O. Downing, F. Chen, P. Zavalij, A. Mun˜oz-Castro, B.W. Eichhorn, Chem. Eur. J. 26 (2020) 5824–5833.
[58] Chemcraft. Available online: http://www.chemcraftprog.com (accessed on 24 April 2023).